Spin-locking in low-frequency reaction yield detected magnetic resonance†

C. J. Wedge,[a,b,‡] Jason C. S. Lau,[b] Kelly-Anne Ferguson,[a] Stuart A. Norman,[a] P. J. Hore*[b] and Christiane R. Timmel,*[a]

Received Xth XXXXXXXXXX 20XX, Accepted Xth XXXXXXXXX 20XX
First published on the web Xth XXXXXXXXXX 200X
DOI: 10.1039/c3cp52019f

The purported effects of weak magnetic fields on various biological systems from animal magnetoreception to human health have generated widespread interest and sparked much controversy in the past decade. To date the only well established mechanism by which the rates and yields of chemical reactions are known to be influenced by magnetic fields is the radical pair mechanism, based on the spin-dependent reactivity of radical pairs. A diagnostic test for the operation of the radical pair mechanism was proposed by Henbest *et al.* [*J. Am. Chem. Soc.*, 2004, **126**, 8102] based on the combined effects of weak static magnetic fields and radiofrequency oscillating fields in a reaction yield detected magnetic resonance experiment. Here we investigate the effects on radical pair reactions of applying relatively strong oscillating fields, both parallel and perpendicular to the static field. We demonstrate the importance of understanding the effect of the strength of the radiofrequency oscillating field; our experiments demonstrate that there is an optimal oscillating field strength above which the observed signal decreases in intensity and eventually inverts. We establish the correlation between the onset of this effect and the hyperfine structure of the radicals involved, and identify the existence of 'overtone' type features appearing at multiples of the expected resonance field position.

1 Introduction

Reactions of spin-correlated radical pairs (SCRPs) are known to be sensitive to the application of weak static and/or oscillating magnetic fields, despite an interaction energy orders of magnitude less than the thermal energy $k_{\mathrm{B}}T$. These surprising effects arise from the spin-dependent nature of radical pair reactions combined with the coherent interconversion of radical pair electron spin states driven by internal and external magnetic interactions. These effects are described by the Radical Pair Mechanism (RPM), the only universally acknowledged mechanism by which weak magnetic fields can influence chemical reactions.[1–3] A diagnostic test for the operation of the RPM is therefore of significant importance to the debates surrounding both the mechanism of avian magnetoreception and the existence of putative human health effects of weak electromagnetic fields. Such a diagnostic test is provided by reaction yield detected magnetic resonance (RYDMR) experiments in which a radiofrequency (RF) oscillating field is combined with a weak (< 4 mT) static magnetic field.[4]

The results presented here demonstrate that if the strength of the RF oscillating field is too great the RYDMR signal intensity may decrease or the signal may invert in a spin-locking phenomenon. A thorough understanding of such processes is essential if RYDMR is to be applied successfully as a diagnostic test for involvement of the RPM. The origin of apparent 'overtone' resonances, occurring at multiples of the Zeeman resonance field, is also explored.

The RPM operates on the SCRPs that are generated as intermediates in a range of photolytic, radiolytic and thermolytic reactions. Conservation of spin angular momentum requires that the correlated electron spins of the radicals share the same multiplicity (singlet or triplet) as their molecular precursor. If the diffusive separation of the radicals is sufficient that the inter-radical exchange and dipolar interactions are comparable to the electron-nuclear hyperfine interactions then the radical pair spin state may oscillate coherently between the singlet and triplet states. The recombination probability from subsequent re-encounters of the radicals depends on the spin state at the instant of collision, singlet recombination more normally being the reactive channel leading to a diamagnetic ground state. If geminate pair encounters do not result in recombination, diffusive separation of the radicals will eventually occur. Crucially, externally applied magnetic fields also affect the interconversion of the various electron spin states thus altering

† Electronic Supplementary Information (ESI) available: Further information on experimental calibration; additional experimental data and spectral simulations. See DOI: 10.1039/c3cp52019f

[a] *Department of Chemistry, University of Oxford, Centre for Advanced Electron Spin Resonance, South Parks Road, Oxford, OX1 3QR, UK. E-mail: christiane.timmel@chem.ox.ac.uk*
[b] *Department of Chemistry, University of Oxford, Physical and Theoretical Chemistry Laboratory, South Parks Road, Oxford, OX1 3QZ, UK. E-mail: peter.hore@chem.ox.ac.uk*
‡ *Present address: Department of Physics, University of Warwick, Gibbet Hill Road, Coventry, CV4 7AL, UK.*

the yield of the singlet product and conferring magnetic sensitivity on the reaction yield. For example, static magnetic fields lift the degeneracy of the triplet substates (T_0, T_+, T_-), corresponding to different projections of the total spin angular momentum, which may hinder interconversion between singlet (S) and $T_\pm$ states. [1–3]

The short lifetimes (typically nanoseconds to microseconds) and low concentrations of radical pairs make direct detection of the radical magnetization in conventional time-resolved EPR (electron paramagnetic resonance) spectroscopy difficult. This problem has been circumvented by utilizing reagents in which photolytic radical generation leads to a magnetically sensitive fluorescence, allowing an optically detected low-field EPR technique to be developed. [4–6]

2 Experimental Methods

All RYDMR experiments were carried out using apparatus similar to that developed previously for investigation of RF polarization effects. [6,7] The reagent solution flowed rapidly in a recirculating loop through a 5 mm optical path-length quartz cuvette, with radical pair generation achieved by photolysis under continuous UV irradiation from a 1 kW arc lamp. The resultant fluorescence signal perpendicular to the irradiation source was collected and focussed onto a photomultiplier tube for detection, with an interference filter used to select exciplex fluorescence in a 100 nm pass band centred at 548 nm.

As in our previous zero- and low-field magnetic resonance studies [6,7] the applied RF oscillating field was amplitude-modulated at 331 Hz, allowing phase-sensitive detection to be used to select for the component of the total fluorescence that depends on the applied RF field. Recorded signals therefore correspond only to the effect of the RF oscillating field which is orders of magnitude weaker than the fluorescence background, and although the effect of the RF fields depends on the static field present, the actual static field effect (relative to true zero field) is not recorded. In contrast to our previous broadband apparatus the system operated at the single frequency of 36 MHz and used a single Helmholtz coil pair to produce only a linearly-polarized RF field. A simple tuned circuit was employed to allow matching of the coil to the 50 Ω output impedance of a 100 W RF amplifier so that high RF field strengths could be obtained. Due to RF heating effects on the electrical properties of the coils, an in-line power meter was used to re-optimize the tuning of the circuit by minimization of reflected power for each input power. The oscillating field strength was monitored continuously using the voltage induced on a small search loop fixed on the same axis as the field-generating coils. Details of the calibration of the oscillating field strength can be found in the ESI.†

Experiments were performed on solutions of chrysene (Chr), pyrene (Py) or their perdeuterated analogues (1 mM) with 1,2-, 1,3- or 1,4-dicyanobenzene (DCB) (20 mM) in 1:9 acetonitrile:cyclohexanol solvent mixture at 20°C. Photoexcitation of Chr or Py generates a singlet excited state which forms an exciplex with DCB. Subsequent electron transfer to DCB generates a radical ion pair exclusively in the singlet state, with back electron transfer and exciplex fluorescence possible only for radicals that re-encounter in the singlet state. RYDMR spectra were obtained at the fixed radiofrequency of 36 MHz with a static magnetic field of up to 4 mT aligned either parallel or perpendicular to the RF oscillating field.

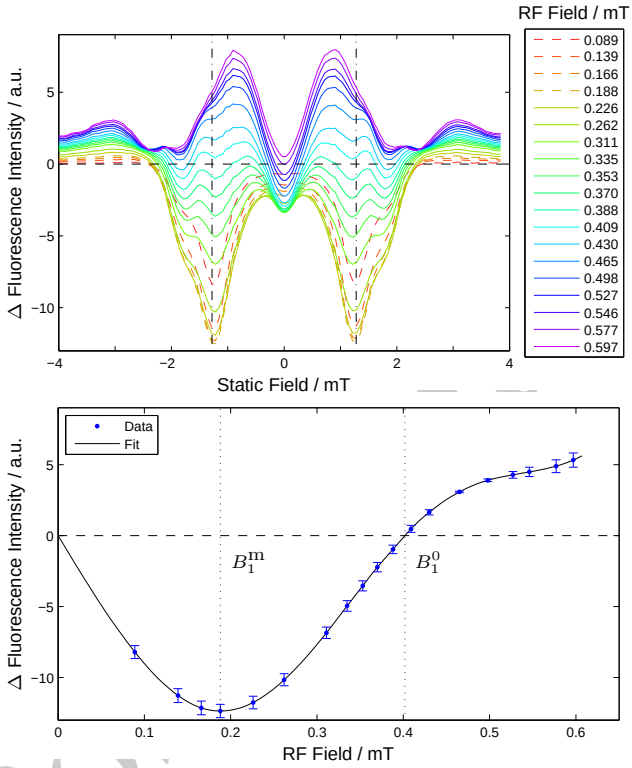

Fig. 1 Experimental RYDMR spectra of Py-d_{10}/1,3-DCB for a 36 MHz oscillating field applied orthogonal to the static field. RYDMR-B_0 (top) and RYDMR-B_1 (bottom) representations are shown for the same data set. For clarity, the RYDMR-B_0 spectra recorded at RF field strengths below B_1^m are given dashed lines. Vertical dot-dashed lines in the top figure indicate the Larmor resonance field at ±1.28 mT; plotting the signal intensity at this static field against RF field strength generates the RYDMR-B_1 spectrum. Vertical dotted lines in the bottom figure indicate the characteristic values B_1^m and B_1^0 (see text for details).

For a fixed alignment of the fields two types of RYDMR spectra can be envisaged: RYDMR-B_0 where the static field strength B_0 is varied, and RYDMR-B_1 in which the root-mean-square oscillating field strength B_1 is altered; in both cases all other parameters are held constant (Fig. 1). In the latter case the static field is conventionally matched to the expected

Zeeman resonance position ($B_0 = 1.28\,\mathrm{mT}$ for $f_{\mathrm{rf}} = 36\,\mathrm{MHz}$). As it is difficult experimentally to vary B_1 continuously all RYDMR-B_1 spectra were obtained by extracting the relevant data points from a series of RYDMR-B_0 spectra recorded for different B_1 field strengths. The strength of the static field could be swept through zero to obtain symmetrical RYDMR-B_0 spectra which were used to correct for a small constant offset in the static field axis produced by the lock-in detection technique.

The phase of the measured spectra was set such that negative signals correspond to decreased exciplex fluorescence, resulting from an RF-induced reduction in the singlet fraction of radical pairs.[5] In the high-field limit one can understand the action of a static magnetic field as inducing a Zeeman splitting that energetically isolates the S and T_0 states from $T_\pm$, hindering their mixing and hence increasing the singlet yield from singlet-born radical pairs. The negative signals conventionally observed in RYDMR thus correspond to a reconnection of these states by a resonant oscillating field in what is known as a spin-pumping transition. As will be shown below, for sufficiently high B_1 a positive signal is observed corresponding to a further increase in singlet yield in addition to that already induced by the static magnetic field; this will be referred to as a spin-locking effect. The action of the RF field in this spin-locking regime is to restrict singlet-triplet interconversion, so it appears as though the oscillating field is "locking" the unpaired spins into the singlet state. An analogous effect is well known in NMR (nuclear magnetic resonance) spectroscopy; in that context the rotating frame magnetization of two spins with different chemical shifts can be locked onto the same rotating frame axis by a strong RF field of suitable phase, preventing mutual dephasing of those spins.[8] In the RYDMR case the two unpaired electron spins are effectively locked to the RF field, remaining in phase with that field and hence one-another, preventing singlet-triplet interconversion.

The onset of spin-locking may be characterised by defining two values of the oscillating field strength: B_1^{m} which is the value giving the most intense spin-pumping signal and B_1^0 at which the singlet yield is identical to that in the absence of an oscillating field, corresponding respectively to the minima and zero-crossing points in RYDMR-B_1 spectra (Fig. 1).

3 Theoretical Methods

3.1 Modulation Effects

In the RYDMR experiments performed, audiofrequency (AF) amplitude modulation of the RF field is used along with lock-in detection to allow the small RF effect to be observed in the presence of a large background. A purpose-built mixing box based on an AD835 4-quadrant multiplier combined the RF signal with the AF reference output of the lock-in amplifier (LIA) giving a maximum modulation depth of 88.5%, which was used in all experiments to maximize signal intensity. If the fluorescence intensity is linear in B_1 the measured signal may be treated as the difference between the singlet yield in the presence and absence of the RF field. It was shown previously for weak oscillating fields that this remains a good approximation despite non-linearities in the B_1 dependence of the singlet yield.[5,9] Examining the RYDMR-B_1 spectra in Fig. 1 it is obvious that as B_1 increases this will become a progressively poorer approximation; for fields comparable to or greater than B_1^0 the signal is effectively averaged between spin-pumping and spin-locking regimes. A technique to demodulate the experimental data to obtain directly the RF-induced change in singlet yield has therefore been developed based on the action of the LIA itself.[9]

After mixing of the RF and AF signals the time-dependence of the B_1 field is as follows:

$$B_1(t) = B_1^{\max} \sin(2\pi f_{\mathrm{RF}} t)\left(1 - M\sin^2(\pi f_{\mathrm{AF}} t)\right) \qquad (1)$$

where f_{RF} is the radiofrequency, f_{AF} is the audiofrequency and M is the fractional modulation depth. This B_1 field affects the radical pair reaction and hence the detected fluorescence signal. The LIA then mixes a cosine function of the same AF as the reference output used to modulate the B_1 field, with this input signal. The result of low-pass filtering is to remove all oscillating signal components with the exception of those at the reference AF which are converted to a direct current signal that is subsequently recorded.[§] We can represent the action of this filtering mathematically as the integral over one modulation period.[10]

We can describe the dependence of the singlet yield, Φ_{S}, on the B_1 field at a particular B_0 field as a polynomial. The simplest polynomial is a linear equation,

$$\Phi_{\mathrm{S}}(B_1) = k_1 B_1 + k_0 \qquad (2)$$

where $k_0 = \Phi_{\mathrm{S}}(0)$ is the singlet yield in the absence of the RF oscillating field. Then the signal output of the LIA is the integral of the product of Eq. 2 and a reference cosine function over one modulation period:

$$s = \int_0^{t_{\mathrm{m}}} \Phi_{\mathrm{S}}(B_1)\cos(2\pi f_{\mathrm{AF}} t)\mathrm{d}t; \qquad t_{\mathrm{m}} = \frac{1}{f_{\mathrm{AF}}}. \qquad (3)$$

The experimentally observed fluorescence signal varies only on the AF timescale hence for our calculation the time-dependence of the B_1 field (Eq. 1) can be simplified by neglecting the high frequency component:

$$B_1(t) = B_1^{\max}\left(1 - M\sin^2(\pi f_{\mathrm{AF}} t)\right). \qquad (4)$$

§ The LIA reference phase is adjusted by the user during calibration experiments to ensure an optimal match between the signal and references phases.

We can now substitute Eq. 4 into Eq. 2, and then into Eq. 3. After evaluating the integral, the signal is:

$$s = \frac{B_1^{\max} M}{4 f_{\mathrm{AF}}}\, k_1. \tag{5}$$

Now substituting Eq. 5 for k_1 in Eq. 2:

$$s = \frac{M}{4 f_{\mathrm{AF}}} \left(\Phi_{\mathrm{S}}(B_1^{\max}) - \Phi_{\mathrm{S}}(0)\right) = \frac{M}{4 f_{\mathrm{AF}}} \Delta\Phi_{\mathrm{S}}. \tag{6}$$

If we assume that the singlet yield is linear in B_1, the output signal is also linear in B_1 (Eq. 5). However looking at the experimental data, the signal is clearly not linear in B_1 (Fig. 1) and therefore we need a higher order polynomial. Although in practice the order n is chosen based on the number of available constraints (see below), for brevity we will take as an example the approximation of the singlet yield as a 4-th order polynomial.

$$\Phi_{\mathrm{S}}(B_1) = k_4 B_1^4 + k_3 B_1^3 + k_2 B_1^2 + k_1 B_1 + k_0 \tag{7}$$

We can now substitute Eq. 4 into Eq. 7, then into Eq. 3 and evaluate the integral:

$$\begin{aligned} s = \frac{1}{f_{\mathrm{AF}}} \Bigg[& k_4 \, \frac{{B_1^{\max}}^4}{2} \left(-\frac{7M^4}{16} + \frac{15M^3}{8} - 3M^2 + 2M \right) \\ & + k_3 \, \frac{{B_1^{\max}}^3}{4} \left(\frac{15M^3}{16} - 3M^2 + 3M \right) \\ & + k_2 \, \frac{{B_1^{\max}}^2}{2} \left(M + \frac{M^2}{2} \right) + k_1 \, \frac{B_1^{\max} M}{4} \Bigg]. \end{aligned} \tag{8}$$

Whatever the order of polynomial used to represent the singlet yield dependence, the signal will also be a polynomial of the same order and go through the origin. Therefore we can use polynomial interpolation of the experimental data to calculate the polynomial coefficients. We can then use the coefficients and Eq. 8 to calculate $k_4, \cdots, k_1$ in Eq. 7 and work out the true singlet yield dependence on B_1:

$$\begin{aligned} \Delta\Phi_{\mathrm{S}}(B_1) &= \Phi_{\mathrm{S}}(B_1) - \Phi_{\mathrm{S}}(0) \\ &= k_4 B_1^4 + k_3 B_1^3 + k_2 B_1^2 + k_1 B_1. \end{aligned} \tag{9}$$

It should be noted that $\Phi_{\mathrm{S}}(0) = k_0$ depends on the static field strength B_0 but is independent of B_1 and is not present in Eq. 9, hence the absolute value of the singlet yield is not determined. The number of coefficients to determine is therefore less than n and is further reduced by applying the constraint $k_1 \leq 0$, which ensures that the gradient of the polynomial does not become positive in the weak-field region where the value of B_1 is below that of the lowest recorded data point.

Finding the polynomial coefficients for a polynomial that goes through or near multiple data points involves solving the set of simultaneous equations in a least-squares sense:

$$\min \|Wx - d\|_2^2 \tag{10}$$

where W is the Vandermonde matrix, x is the vector of the polynomial coefficients and d are the experimental data to be interpolated. One major problem in solving Eq. 9 is that for a high-order polynomial, W is ill-conditioned. In order to calculate a meaningful solution to Eq. 9, we need to add regularisation to the equation:

$$\min \|Wx - d\|_2^2 + \|\lambda L x\|_2^2 \tag{11}$$

where L is a suitably chosen Tikhonov matrix and λ is the regularisation parameter. We have chosen L to be the identity matrix so as to minimise the 2-norm of the polynomial coefficients. λ is chosen to be 0.0005 which adds enough regularisation that the problem has a meaningful solution and the least squares semi-norm has the same magnitude as the expected experimental error. The order n of the polynomial used to fit the data was picked to be one less than the number of experimentally measured RF field strengths, meaning that $n-1$ coefficients were obtained by a constrained fit to $n+1$ data points. Examination of plots of $k_n, \cdots, k_1$ against B_0 (not shown) verifies that these parameters are well-behaved.

3.2 Simulation Methods

Having removed the effects of signal modulation from the experimental data it is possible to compare them directly with numerical simulations performed without the computational expense of integrating over a full modulation cycle of the RF field. Using a simple subtraction method our simulations find the difference in singlet yield at a given RF field strength relative to $B_1 = 0$, at all times in the presence of the static field B_0.[5] In the high-field limit it is convenient to make the rotating frame approximation in order to remove the time-dependence of the problem. Such an approximation cannot be used in the low-field limit[6] or when the static and oscillating fields are not orthogonal. A modified form of the γ-COMPUTE algorithm[11–13] is used which exploits the periodicity of the problem and efficiently averages over the initial phase of the RF field.[5] For each radical the group of equivalent nuclei with the largest isotropic hyperfine coupling was included in the simulations. The effective hyperfine coupling of each radical is defined as:

$$a_{\mathrm{eff}} = \sqrt{\sum_k a_k^2 I_k (I_k + 1)} \tag{12}$$

where the sum is over all nuclei k with hyperfine coupling a_k and nuclear spin quantum number I_k. For the radical pair (R1, R2) we compute:

$$a_{\mathrm{RP}} = \sqrt{a_{\mathrm{eff,R1}}^2 + a_{\mathrm{eff,R2}}^2} \tag{13}$$

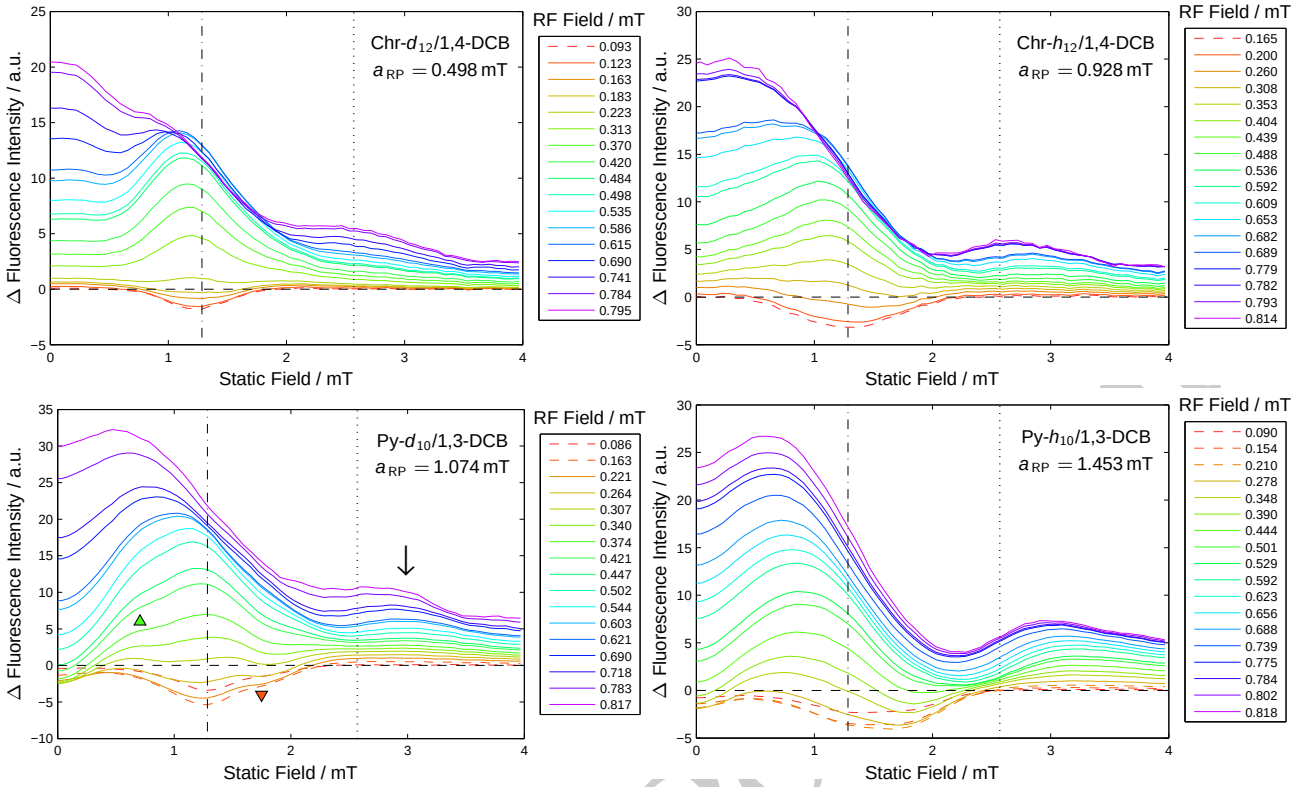

Fig. 2 Experimental RYDMR-B_0 spectra of various exciplex systems as indicated, for a 36 MHz oscillating field applied orthogonal to the static field. For clarity, the spectra recorded at RF field strengths below B_1^{m} are given dashed lines. Vertical lines indicate the Larmor resonance field at 1.28 mT (dot-dashed line) and twice the Larmor resonance field at 2.56 mT (dotted line). Symbols ▲, ▼ and ↓ indicate spectral features described in the text.

Table 1 Effective hyperfine coupling constants in mT for radical pairs formed by the electron donors and acceptors used in this study, calculated from literature values [16–19] using Eq. 13. When data for the deuterated compound was not available the hyperfine coupling was estimated from that of the protonated radical using $a_{\mathrm{H}}/a_{\mathrm{D}} \approx \gamma_{\mathrm{H}}/\gamma_{\mathrm{D}} = 6.51$.

Radical	1,2-DCB$^{\bullet-}$	1,3-DCB$^{\bullet-}$	1,4-DCB$^{\bullet-}$
chrysene-$h_{12}^{\bullet+}$	1.018	1.320	0.928
chrysene-$d_{12}^{\bullet+}$	0.650	1.063	0.498
pyrene-$h_{10}^{\bullet+}$	1.185	1.453	1.109
pyrene-$d_{10}^{\bullet+}$	0.667	1.074	0.521

resulting in the values given in Table 1. The radicals were assumed to encounter with an exponential probability distribution, $f(t) = k\exp(-kt)$ where k^{-1} is the radical pair lifetime. In this often used 'exponential model' [14,15] radicals are assumed to encounter only once and react with the probability of their being in the singlet state at the time of encounter.

4 Results

4.1 RYDMR-B_0–orthogonal fields

Spectra for orthogonal field-orientations were collected for ten related exciplex systems to identify the effects of systematically varying the hyperfine coupling constants. Representative RYDMR-B_0 spectra are shown in Fig. 2 for the Py/1,3-DCB and Chr/1,4-DCB systems with protonated and deuterated isotopomers of the electron donor (Further spectra are shown in the ESI†). Looking first at the Py-d_{10}/1,3-DCB system, for the lowest RF field strength a negative resonance is observed, centred at $B_0 = 1.28$ mT, as expected for a 36 MHz field according to the normal EPR resonance condition (28 MHz per mT). This corresponds to a decrease in singlet yield with respect to application of the static field alone, and may be rationalised in the normal way as a reconnection of Zeeman-split S/T_0 and $T_{\pm}$ states. With increasing RF field strength the signal intensity initially increases (becomes more negative) corresponding to an increase in mixing efficiency. For field strengths above $B_1 \approx 0.17$ mT (solid lines) the signal intensity decreases again,

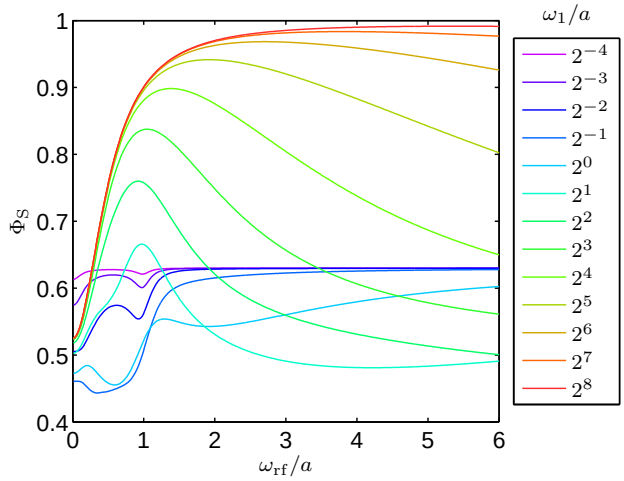

Fig. 3 Rotating frame OMFE simulation for a one-proton radical pair, hyperfine coupling a. The resonance at $\omega_{rf}/a = 1$ is inverted and broadened as the RF field strength is increased. The abscissa and legend give the frequency, ω_{rf}, and strength, ω_1, of the RF field, both scaled by the hyperfine coupling constant a.

indicating that the efficiency of singlet-triplet mixing is being reduced by the strong RF field. As B_1 reaches 0.3 mT there is a clear inversion in the central part of the resonance, as was seen in previous X-band RYDMR studies of the same system.[20] This is in contrast to studies of photosynthetic systems, in which the wing portions inverted first.[21] With further increase in B_1 the whole signal is inverted, with shoulders arising from unresolved hyperfine couplings observed (indicated by ▲ in Fig. 2), just as in the spectra at low RF field strengths (indicated by ▼ in Fig. 2). Whereas in the high-field limit the hyperfine structure ought to be symmetrical the line shape at 36 MHz is asymmetric; for weak RF fields the hyperfine structure is better resolved on the high static field side of the resonance as noted previously,[6] whereas for stronger RF fields the shoulder on the weak static field side is better resolved.

For sufficiently large RF field strengths a second, positive, resonance feature appears at around $B_0 = 3.0$ mT (indicated by an arrow in Fig. 2). The possibility that this is the result of an amplifier harmonic was excluded by the insensitivity of the feature to the insertion of RF filters. A passive filter on the amplifier output provided 42 dB attenuation and an active filter on the amplifier input provided 25 dB attenuation at 72 MHz with respect to the desired 36 MHz output. The origin of this effect will be discussed below in relation to the parallel alignment spectra.

Looking now at the chrysene systems in Fig. 2 the resonances at $B_0 = 1.28$ mT are less structured, and for both Chr isotopomers invert from spin-pumping to spin-locking as expected without any significant shift in resonance position. By contrast in the Py-h_{10}/1,3-DCB case the significantly broader resonance inverts more rapidly on the low-field side, giving rise to an apparent shift in the resonance position. Such behaviour probably arises because in this case the effective hyperfine coupling of the radical pair $a_{RP} = 1.453$ mT (Table 1) is greater than the static field at resonance with the Zeeman interaction, hence conceptual pictures based on the high-field model once again break down at the low static fields of our experiments. There is also an apparent difference at zero static field, which corresponds to the so-called oscillating magnetic field effect (OMFE),[22] a positive signal being observed as B_1 is increased for all systems but a negative signal being seen at low B_1 for the Py/1,3-DCB systems only.

Frequency-swept OMFE (or zero-field EPR) spectra have been shown previously to exhibit resonance features when the frequency of the oscillating field matches the effective hyperfine coupling of either radical partner.[23] Even at zero static field a resonant oscillating field drives singlet-triplet interconversion, hence further reducing the singlet yield from its zero static field value. From previously published OMFE spectra of the Py-d_{10}/1,3-DCB system,[7] it is clear that OMFE spectra of these systems are relatively broad meaning a 36 MHz oscillating field will fall within the resonance feature arising from 1,3-DCB$^{\bullet}$, $a_{eff} = 29.2$ MHz. A corresponding decrease in singlet yield is therefore observed at $B_0 = 0$ in the RYDMR spectra of Py/1,3-DCB systems whereas for Chr/1,4-DCB the 36 MHz field is too far from the nearest resonant frequency (Chr-$h_{12}^{\bullet+}$, $a_{eff} = 22.7$ MHz) to generate an effect for a weak B_1 field. Despite the poor frequency match to the effective hyperfine couplings of the radical partners a sufficiently strong RF field produces a positive OMFE signal. Using a simple rotating frame simulation Fig. 3 shows that this arises due to inversion and significant broadening of the OMFE signal for sufficiently strong RF field strengths, such that singlet-triplet interconversion is effectively blocked even far from resonance.

4.2 RYDMR-B_1–orthogonal fields

For all systems studied RYDMR-B_1 spectra were obtained and B_1^0 values extracted as described above. Plotting B_1^0 against the effective hyperfine coupling constant gives an approximately linear dependence, Fig. 4. It seems reasonable that a stronger RF field would be required to spin-lock a system with a larger hyperfine coupling constant, though previous higher field work did not suggest a linear relationship.[20] Based upon a one-proton radical pair model, the relation,

$$B_1^0/a = c\sqrt{a\tau} \tag{14}$$

with $c \approx 0.2$, a the hyperfine coupling and $\tau = k^{-1}$ the radical pair lifetime, was suggested by Batchelor.[20] It appears from the data presented here that such a relation does not hold, at least in the low-field limit when applying a 36 MHz field. In

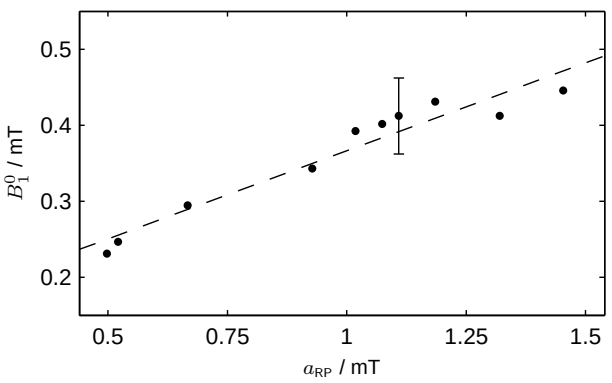

Fig. 4 Variation in B_1^0 with the effective hyperfine coupling of the radical pair as calculated using Eq. 13 and given in Table 1. A representative error bar shows the estimated accuracy of ± 0.05 mT in the determination of B_1^0.

the rotating frame vector model proposed by Koptyug *et al.*[24] the singlet-triplet mixing rate ω_{ST} is given by $\omega_{ST} \approx \Delta\omega$ when $\omega_1 \ll \Delta\omega$ and $\omega_{ST} \approx \Delta\omega^2/2\omega_1$ when $\omega_1 \gg \Delta\omega$, where $\Delta\omega$ is the difference in spin-precession rates caused by differences in the hyperfine coupling constants of the two radicals. The value of B_1^0 corresponds to the B_1 field strength at which ω_{ST} equals that for zero oscillating field. Taking the zero-field mixing rate as $\Delta\omega$ and equating with the rate for a strong RF field gives $\Delta\omega = 2\omega_1$ as the condition for equal mixing rates. A linear dependence of B_1^0 on $\Delta\omega$ is therefore predicted, though the numerical factor is incorrect. It should also be noted that the derivation uses the difference in precession frequencies, whereas we are using the effective hyperfine coupling constant of the entire radical pair. Correlation with the difference in a_{eff} of the two radical partners was not observed ($r < 0.3$).

The onset of spin-locking appears at a surprisingly low RF field strength. It was proposed that an optically-detected EPR signal should invert when the field amplitude B_1 exceeds the spectral width,[24] yet here it has been shown that a field much weaker than the effective hyperfine coupling constant of the radical pair may cause such an inversion. This result while unexpected is in reasonable agreement with γ-COMPUTE simulations (not shown), the onset of spin-locking depending upon both the hyperfine structure and radical pair recombination kinetics.

According to Eq. 14 the onset of spin-locking ought to depend upon radical pair lifetime as well as the effective hyperfine coupling of the radical pair. A systematic variation of radical pair lifetime through alteration of the radical recombination rate is difficult to achieve experimentally, however the nuclear spin configuration lifetime depends on the rate of degenerate electron exchange (DEE), which is proportional to the concentration of the diamagnetic form of the exchanging species. In the case of static magnetic field effects (Magnetically Altered Reaction Yields, MARY), changes in the characteristic $B_{1/2}$ values of the spectra have been used to monitor degenerate electron exchange rates of DCB radical anions.[25] This effect arises from uncertainty broadening associated with reduced nuclear spin configuration lifetimes, the hyperfine couplings of the exchanging radical averaging to zero in the fast-exchange limit. DEE gives rise to similar effects in RYDMR, with changes in B_1^0 values observed as the DCB concentration is varied. Previous studies of DEE using X-band RYDMR were limited to weak B_1 fields and hence only able to demonstrate alteration in RYDMR-B_0 lineshape.[20] As seen in Fig. 2 our RF field strengths are sufficient to fully invert the 36 MHz RYDMR signal to obtain B_1^0 values hence we could plot the change in B_1^0 from slow to fast exchange limits (see ESI†). A potential advantage of RYDMR over MARY is that the sensitivity of B_1^0 could be tuned to a particular range of electron exchange rates through careful choice of the frequency of the B_1 field. Although confirmed by preliminary simulations in the rotating frame this possibility has not yet been fully explored owing to the high computational cost of simulating the effects of linearly-polarized oscillating magnetic fields combined with degenerate electron exchange effects.

4.3 Orientation-dependent effects

In the low-frequency regime even weak radiofrequency fields are able to induce a resonance when applied parallel to a static field, contrary to high-field selection rules.[4–6] The breakdown of high-field models is gradual, parallel transitions becoming significant at higher frequencies than those at which the rotating frame approximation breaks down.[6] Extending previous studies, orientation effects are now investigated in the case of strong B_1 fields. According to the model proposed by Koptyug *et al.*[24] for spin-locking it should not be possible to cause a spin-locking type inversion for parallel fields, an assertion that is tested below, alongside discussion of higher order resonances.

To describe the main features observed it is helpful to compare directly the parallel and perpendicular orientations at the same RF field strength, as in Fig. 5. For $B_1 \approx 0.1$ mT both orientations give rise to a spin-pumping signal close to the Zeeman resonance condition $B_0 = 1.28$ mT, corresponding to increased singlet-triplet mixing with respect to application of the static field alone. This resonance is weaker in the case of the parallel orientation, and significantly broadened towards higher static field strengths. At zero static field the two spectra ought to coincide, regardless of radiofrequency field strength, as both correspond to the OMFE. Due to minor changes in optical alignment and sample concentration the total fluorescence intensity varied slightly between experimental runs col-

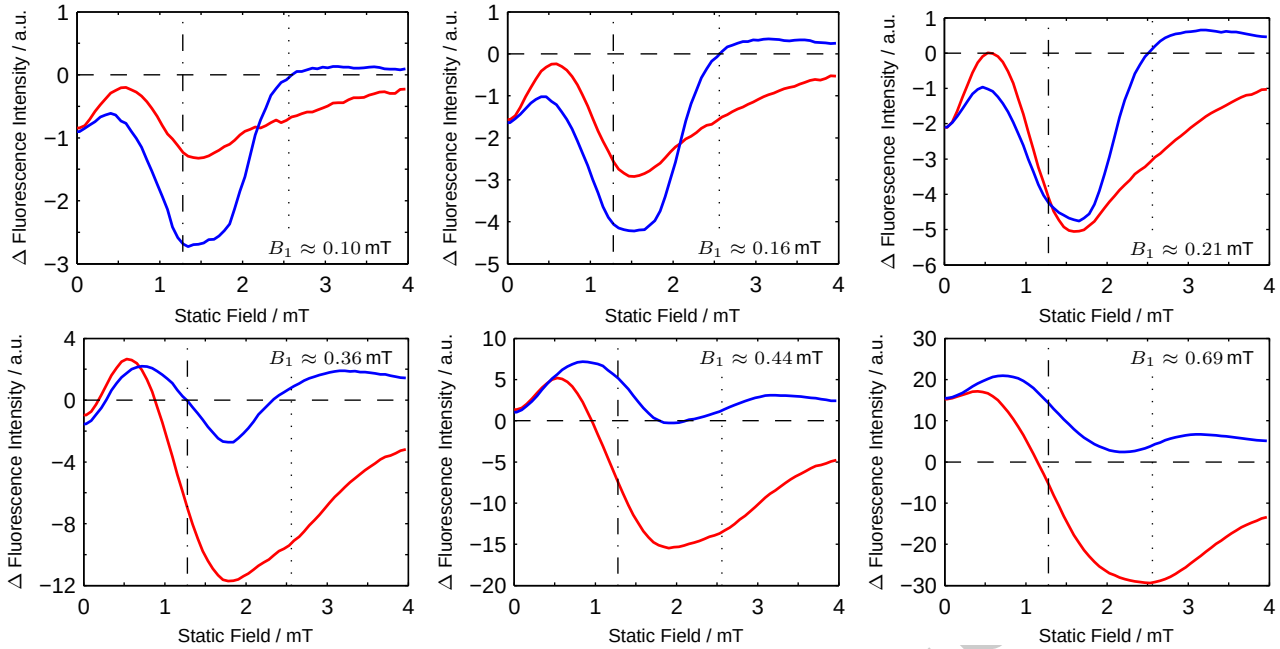

Fig. 5 Experimental RYDMR-B_0 spectra of the Py-h_{10}/1,3-DCB system comparing parallel (red) and perpendicular (blue) orientations of static and RF fields, at different RF field strengths as indicated. Although the same RF powers were used for each pair of spectra it should be noted that the measured RF field strength is only approximately equal in each case due to coil heating effects. Vertical lines indicate the Larmor resonance field at 1.28 mT (dot-dashed line) and twice the Larmor resonance field at 2.56 mT (dotted line).

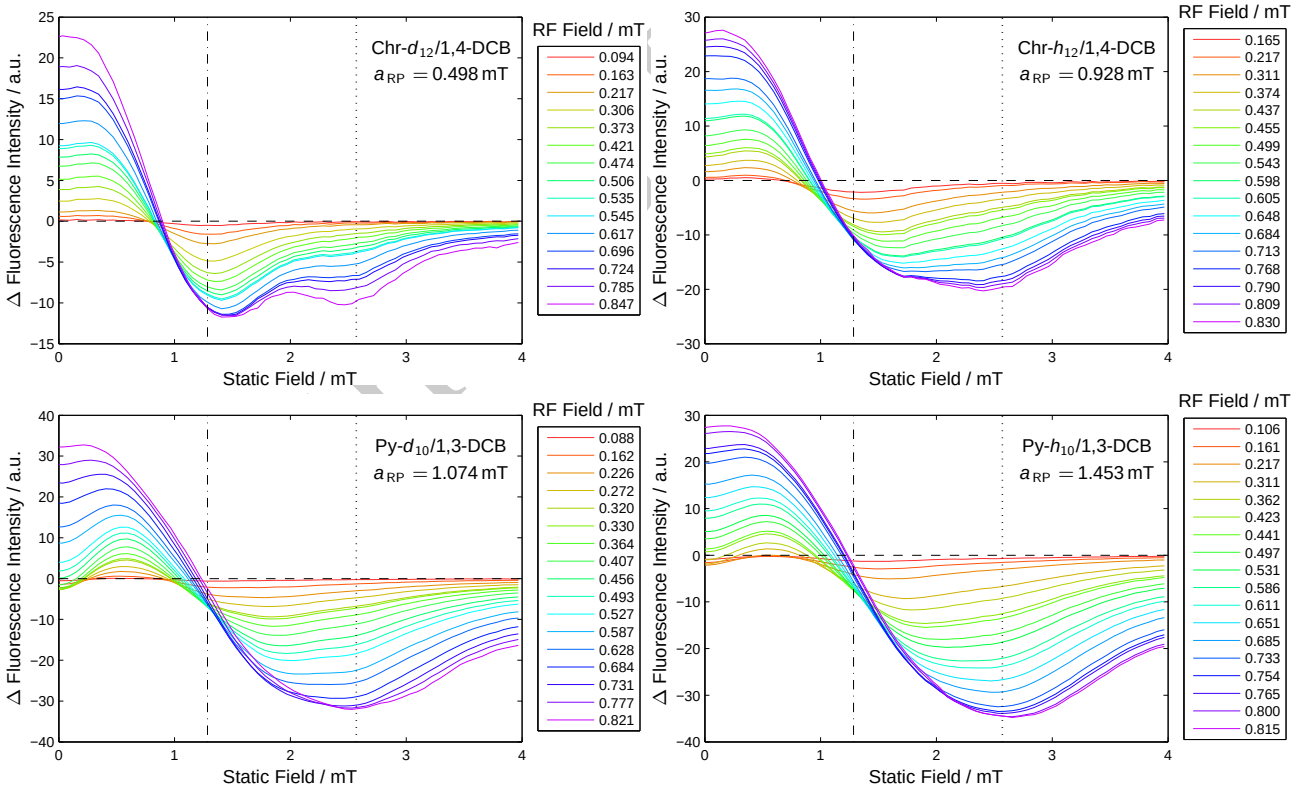

Fig. 6 Experimental RYDMR-B_0 spectra of various exciplex systems as indicated, for a 36 MHz oscillating field applied parallel to the static field. Vertical lines indicate the Larmor resonance field at 1.28 mT (dot-dashed line) and twice the Larmor resonance field at 2.56 mT (dotted line).

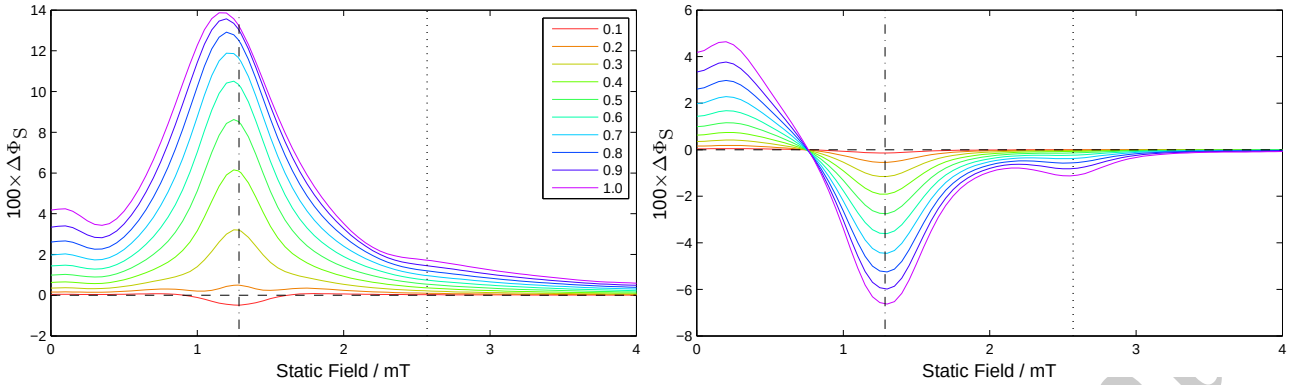

Fig. 7 Simulated RYDMR-B_0 spectra of the Chr-$d_{12}^{\bullet+}$/1,4-DCB$^{\bullet-}$ system, calculated using γ-COMPUTE with nuclei Chr-$d_{12}^{\bullet+}$ $2D \times 0.085\,\mathrm{mT}$; 1,4-DCB$^{\bullet-}$ $4H \times 0.159\,\mathrm{mT}$, $k = 3 \times 10^7\,\mathrm{s}^{-1}$. The RF field strength in mT is given in the legend. Vertical lines indicate the Larmor resonance field at 1.28 mT (dot-dashed line) and twice the Larmor resonance field at 2.56 mT (dotted line).

lected at different orientations, therefore a small scaling factor was applied to all parallel data based upon the mean ratio of signal intensities at zero static field.

As B_1 is increased the relative intensities of the two signals switch, such that the parallel orientation gives the strongest resonance, even at $B_1 \approx 0.21\,\mathrm{mT}$ which is close to B_1^{m} for this system, the RF field strength at which the perpendicular orientation gives the maximum spin-pumping signal. Further increase in B_1 leads to a steady increase in the intensity of the resonance in the parallel case, with a shift toward higher static field strengths. At the maximum available RF field strength there has been no inversion of the parallel signal, in accordance with the postulate by Koptyug *et al.*[24] A positive signal does, however, emerge at around $B_0 = 0.5\,\mathrm{mT}$, a significantly lower field than the spin-locked resonance in the perpendicular case.

Previous studies have shown that in most RYDMR spectra there is a static field value at which the RYDMR signal is independent of the angle θ between the static and oscillating fields.[5,6] Numerical simulations using the γ-COMPUTE algorithm indicate that this θ-independent point shifts to lower static fields as B_1 increases, as indeed is observed in Fig. 5 with a shift from $B_0 \approx 2.2\,\mathrm{mT}$ for $B_1 = 0.10\,\mathrm{mT}$ to $B_0 \approx 1.3\,\mathrm{mT}$ for $B_1 = 0.21\,\mathrm{mT}$. Simulations also indicate that a shift to lower static field will be seen as the radical pair lifetime decreases, hence the B_1 dependence of a series of RYDMR-B_0 spectra may be used to estimate the RP lifetime. Unfortunately a systematic variation of radical pair lifetime is not trivial experimentally; our attempts to do so using micellar solutions suffered from poor signal to noise, but did indicate a $\sim$1.6 fold increase in lifetime for Py-h_{10}/1,3-DCB upon increase of surfactant chain length from dodecyl- to hexadecyltrimethylammonium chloride (data in ESI†).

Looking at the spectra for strong radiofrequency fields ($B_1 > 0.4\,\mathrm{mT}$) in Fig. 5 a second broad spin-locked resonance is observed in the perpendicular case. This is at a higher static field strength than would be expected if this was some form of two-photon process, a field of $B_0 = 2.56\,\mathrm{mT}$ being anticipated for any effect of this type. However, a minor shoulder at approximately this location is observed in the parallel case. For further interpretation it is helpful to look to systems with smaller hyperfine couplings, which can be expected to produce sharper resonances. The data collected for four different systems for perpendicular and parallel orientations are shown in Figs. 2 and 6 respectively ordered by a_{RP}. In all cases the negative resonance in the parallel case is seen to shift towards higher static field strengths as B_1 is increased. The apparent shoulder that forms at around $B_0 = 2.56\,\mathrm{mT}$ becomes the dominant resonance in all but the Chr-d_{12}/1,4-DCB case, for which a well resolved shoulder is observed at the highest radiofrequency field strengths. This may be understood in terms of the small effective hyperfine coupling in this system of $a_{\mathrm{RP}} = 0.498\,\mathrm{mT}$ (Table 1). The opposite effect is observed in the perpendicular case (Fig. 2), with the secondary resonance being less well resolved in the case of small hyperfine couplings, despite the sharpening of the Zeeman resonance.

The additional resonances observed for strong radiofrequency fields cannot easily be rationalised in a pictorial manner in either the parallel or perpendicular case. The variation with hyperfine coupling constant of the separation between these resonances and those close to the expected Zeeman resonance position suggests that they may be related to unresolved hyperfine couplings. There is no clear match to any hyperfine splitting in these systems though, the separation between the apparent resonance features being much greater than the largest splitting even in systems using 1,3-DCB which has the largest coupling of 0.829 mT. It is tempting to discuss the additional resonances as two-photon processes within perturba-

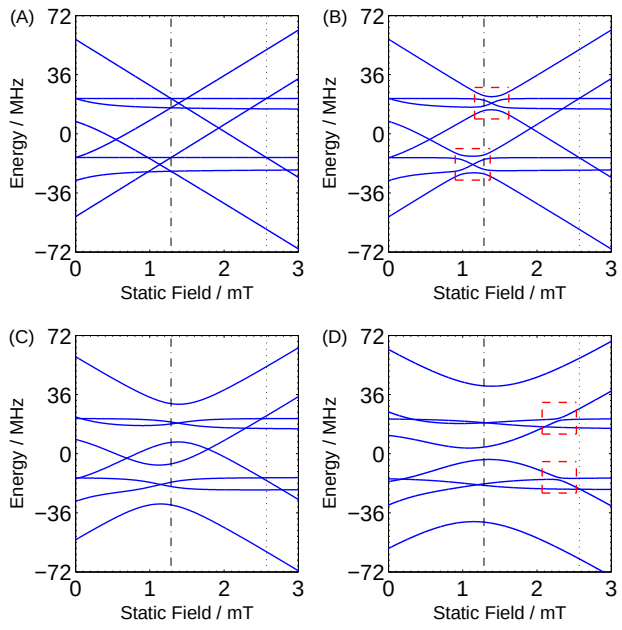

Fig. 8 Rotating frame energy levels for a one-proton radical pair with hyperfine coupling 0.5 mT under the influence of a 36 MHz RF field, with RF field strengths B_1: (A) 0; (B) 0.1 mT; (C) 0.4 mT ; (D) 0.8 mT. Vertical lines indicate the Larmor resonance field at 1.28 mT (dot-dashed line) and twice the Larmor resonance field at 2.56 mT (dotted line). Boxes highlight the appearance of avoided crossings.

tion theory. In this case a perturbation approach is not possible, it being far from clear which of the static, radiofrequency and hyperfine fields might be considered dominant, and which ought to be treated as a perturbation. It may be expected that a linear correlation would be observed between signal intensity for a process of order x and $(B_1)^x$, however we found no evidence for this type of correlation. This is in contrast to previous results at 100 MHz, in which third-order resonances were identified in this manner.[26]

It is clear that in the low-frequency regime the spin-dynamics are complex, yet numerical simulations using the γ-COMPUTE algorithm are able to reproduce the additional resonances (Fig. 7), confirming that they are not an experimental artefact. Performing such simulations for the case of an exceptionally long lived radical pair decreases the linewidth of the resonances, allowing a clearer picture of the underlying structure. For parallel static and oscillating fields, resonances are predicted at $B_0 = 1.28$, 2.56 and 3.84 mT, corresponding to the Larmor resonance positions for 36, 72 and 108 MHz fields. In the perpendicular case even for a long-lived radical pair the additional resonances do not correlate well with the aforementioned static field positions, indicating a shift towards zero static field of the spin-locked resonance. It seems obvious to draw an analogy with the Bloch-Siegert shift, the correction required when treating a linearly-polarized oscillating field as circularly-polarized, which is typically negligible in the high-field limit.[27] The usual derivation gives a shifted resonance position,

$$B'_{\mathrm{res}} = B_{\mathrm{res}}\left(1 - \frac{1}{16}\left(\frac{B_1}{B_0}\right)^2\right) \qquad (15)$$

where B_{res} is the unshifted resonance position. This clearly gives a larger shift for smaller static fields, whereas in the RYDMR case the shift appears to be larger for higher static fields.

In the case of perpendicular fields a simple rotating frame model may be used to gain further insight, although the results obtained must be treated with caution as the neglect of the off-resonance rotating component of the RF field is not fully justified in the low-field regime.[6] The energy levels for a one-proton radical pair in a 36 MHz circularly-polarized field are shown as a function of B_0 in Fig. 8 for various RF field strengths. In relation to the normal Zeeman resonance ($\omega_0 = \omega_{\mathrm{rf}}$) it can be seen that there are a number of level crossings for $B_1 = 0$, which are symmetric about this static field position. These become avoided crossings once the oscillating field is switched on with the separation of the levels increasing as the applied field strength is increased. A second pair of level crossings are seen for $\omega_0 = 2\omega_{\mathrm{rf}}$ when $B_1 = 0$. As the RF field strength is increased these crossings shift to a lower static field strength, but only when $\omega_1 > \omega_{\mathrm{rf}}/2$ does the energy separation at the avoided crossings increase significantly. It is these avoided crossings that are responsible for the secondary resonance seen at a static field position close to twice the Zeeman frequency. This is the same avoided crossing that is responsible for the resonance when $\omega_1 = \omega_{\mathrm{rf}}$, leading to a second predicted minimum in RYDMR-B_1 spectra (not shown), hence it is predicted that should sufficiently strong B_1 fields be available experimentally the apparent secondary resonance feature in the RYDMR-B_0 spectra would shift from $\omega_0 = 2\omega_{\mathrm{rf}}$ to $\omega_0 = \omega_{\mathrm{rf}}$ as B_1 is increased. There are no level crossings for $\omega_0 = 3\omega_{\mathrm{rf}}$ in this simple example with a coupling to a single $I = \frac{1}{2}$ nucleus, but substitution of an $I = 1$ nucleus immediately increases the number of levels, giving a crossing at this position, and increasing the number of crossings for $\omega_0 = \omega_{\mathrm{rf}}$ and $\omega_0 = 2\omega_{\mathrm{rf}}$ (simulations not shown). It can easily be imagined that in the case of a large spin system as encountered in the experimentally observed systems there ought to be a huge number of crossings extending out to many multiples of the frequency of the oscillating field, though their spectral importance will depend on the relative singlet character of the states. Unfortunately such an analysis in the case of parallel static and oscillating fields or linearly-polarized oscillating fields is not trivial.

5 Conclusions

We have shown that RF RYDMR spectra are remarkably sensitive to RF field strength, with spin-locking effects demonstrated even for oscillating fields significantly weaker than the internal electron-nuclear hyperfine interactions. For moderate RF field strengths significant changes in singlet yield were observed without the need for the conventional orthogonal arrangement of static and oscillating fields, at static fields relatively far from the expected Zeeman resonance position and also at zero static field. The sensitivity of the RF field strength and orientation dependencies of the spectra to the underlying radical pair lifetime and hyperfine characteristics demonstrate the potential power of the technique to delineate the properties of the radical pair under investigation. Comparison with numerical simulations will be essential to obtain quantitative information from such studies, being the only available technique for the interpretation of the complex spin-dynamics observed in low-frequency RYDMR.

The complexity of the observed spectra highlight the importance of a full understanding of the competing factors responsible for RYDMR when applying the technique as a diagnostic test for the radical pair mechanism. A number of *in vivo* RYDMR studies have been carried out on birds [28–30] and insects [31] in order to determine the origin of their magnetic sensitivity. These studies provide only a qualitative indication of the RF response: either the RF field produces a statistically significant response or it does not, making it difficult to verify that the observed effects arise from a radical pair mechanism. Attempts have been made to prove a resonance response by finding the threshold RF field strength when on and off resonance with a static field: [30,31] based on the spin-locking phenomena we now propose a definitive test. Applying an on-resonance RF field orthogonal to the static field we can expect an RF response to appear when a threshold RF field strength is exceeded and that this response will disappear again at a higher RF field strength as the radical pair becomes spin-locked and the net RF effect decreases as B_1^0 is approached. When static and RF fields are parallel spin-locking is not possible, though broadening of the OMFE may produce a similar effect, albeit with an onset at higher RF field strength. It is hard to imagine how such a characteristic response could arise by any other mechanism, and as the onset of spin-locking depends on the hyperfine coupling of the radical pair some additional information on the radicals involved could be obtained. Due to the high RF field strengths required and the difficulties in generating these over a large volume, such an experiment may be impractical with birds but ought to be possible with smaller organisms such as fruit fly larvae. [32]

Acknowledgements

We are grateful to the Engineering and Physical Sciences Research Council, The EMF Biological Research Trust and DARPA (QuBE: N66001-10-1-4061) for financial support. We thank Peter Styles and Nick Soffe for advice on RF circuitry, Neville Baker for construction of the RF circuit, and Chris Rodgers and Jonathan Storey for helpful discussions.

References

1 B. Brocklehurst, *Chem. Soc. Rev.*, 2002, **31**, 301–311.
2 U. E. Steiner and T. Ulrich, *Chem. Rev.*, 1989, **89**, 51–147.
3 C. T. Rodgers, *Pure Appl. Chem.*, 2009, **81**, 19–43.
4 K. B. Henbest, P. Kukura, C. T. Rodgers, P. J. Hore and C. R. Timmel, *J. Am. Chem. Soc.*, 2004, **126**, 8102–8103.
5 C. T. Rodgers, K. B. Henbest, P. Kukura, C. R. Timmel and P. J. Hore, *J. Phys. Chem. A*, 2005, **109**, 5035–5041.
6 C. J. Wedge, C. T. Rodgers, S. A. Norman, N. Baker, K. Maeda, K. B. Henbest, C. R. Timmel and P. J. Hore, *Phys. Chem. Chem. Phys.*, 2009, **11**, 6573–6579.
7 C. T. Rodgers, C. J. Wedge, S. A. Norman, P. Kukura, K. Nelson, N. Baker, K. Maeda, K. B. Henbest, P. J. Hore and C. R. Timmel, *Phys. Chem. Chem. Phys.*, 2009, **11**, 6569–6572.
8 M. H. Levitt, *Spin Dynamics: Basics of Nuclear Magnetic Resonance*, Wiley, 2001.
9 C. T. Rodgers, *DPhil Thesis*, University of Oxford, 2007.
10 Stanford Research Systems, *About Lock-in Amplifiers: Application Note 3*.
11 M. H. Levitt and M. Edén, *Mol. Phys.*, 1998, **95**, 879–890.
12 M. Hohwy, H. Bildsøe, H. J. Jakobsen and N. C. Nielsen, *J. Magn. Reson*, 1999, **136**, 6–14.
13 P. Hodgkinson and L. Emsley, *Prog. Nucl. Magn. Reson. Spectrosc.*, 2000, **36**, 201–239.
14 C. R. Timmel, U. Till, B. Brocklehurst, K. A. McLauchlan and P. J. Hore, *Mol. Phys.*, 1998, **95**, 71–89.
15 R. Kaptein and J. L. Oosterhoff, *Chem. Phys. Lett.*, 1969, **4**, 195–197.
16 H. Ohya-Nishiguchi, *Bull. Chem. Soc. Jpn.*, 1979, **52**, 2064–2068.
17 P. H. Rieger and G. K. Fraenkel, *J. Chem. Phys.*, 1962, **37**, 2795–2810.
18 I. C. Lewis and L. S. Singer, *J. Chem. Phys.*, 1965, **43**, 2712–2727.
19 H. Landolt and R. Börnstein, *Landolt-Bornstein physikalisch-chemische Tabellen*, Springer-Verlag, Berlin, 6th edn., 1950.
20 S. N. Batchelor, K. A. McLauchlan and I. A. Shkrob, *Mol. Phys.*, 1992, **75**, 501–529.
21 W. Lersch, F. Lendzian, E. Lang, R. Feick, K. Möbius and M. E. Michel-Beyerle, *J. Magn. Reson*, 1989, **82**, 143–149.
22 C. R. Timmel and P. J. Hore, *Chem. Phys. Lett.*, 1996, **257**, 401–408.
23 J. R. Woodward, C. R. Timmel, K. A. McLauchlan and P. J. Hore, *Phys. Rev. Lett.*, 2001, **87**, 077602/1–4.
24 A. V. Koptyug, V. O. Saik, O. A. Anisimov and Yu. N. Molin, *Chem. Phys.*, 1989, **138**, 173–178.
25 M. Justinek, G. Grampp, S. Landgraf, P. J. Hore and N. N. Lukzen, *J. Am. Chem. Soc.*, 2004, **126**, 5635–5646.
26 V. A. Morozov, O. N. Antzutkin, A. V. Koptyug and A. B. Doktorov, *Mol. Phys.*, 1991, **73**, 517–540.
27 F. Bloch and A. Siegert, *Phys. Rev.*, 1940, **57**, 522–527.
28 T. Ritz, P. Thalau, J. B. Phillips, R. Wiltschko and W. Wiltschko, *Nature*, 2004, **429**, 177–180.
29 P. Thalau, T. Ritz, K. Stapput, R. Wiltschko and W. Wiltschko, *Naturwissenschaften*, 2005, **92**, 86–90.

30 T. Ritz, R. Wiltschko, P. J. Hore, C. T. Rodgers, K. Stapput, P. Thalau, C. R. Timmel and W. Wiltschko, *Biophys. J.*, 2009, **96**, 3451–3457.
31 M. Vácha, T. Půžová and M. Kvíčalová, *J. Exp. Biol.*, 2009, **212**, 3473–3477.
32 M. S. Painter, D. H. Dommer, W. W. Altizer, R. Muheim and J. B. Phillips, *J. Exp. Biol.*, 2013, **216**, 1307–1316.

